



HAL
open science

Thermodynamic and structural properties of lipid-photosensitizer conjugates mixed with phospholipids: Impact on the formation and stability of nano-assemblies

David Chapron, Jean-Philippe Michel, Philippe Fontaine, Jérémy Godard, Frédérique Brégier, Vincent Sol, Véronique Rosilio

► To cite this version:

David Chapron, Jean-Philippe Michel, Philippe Fontaine, Jérémy Godard, Frédérique Brégier, et al.. Thermodynamic and structural properties of lipid-photosensitizer conjugates mixed with phospholipids: Impact on the formation and stability of nano-assemblies. *Colloids and Surfaces B: Biointerfaces*, 2023, 231, pp.113565. 10.1016/j.colsurfb.2023.113565 . hal-04237933

HAL Id: hal-04237933

<https://hal.science/hal-04237933>

Submitted on 11 Oct 2023

HAL is a multi-disciplinary open access archive for the deposit and dissemination of scientific research documents, whether they are published or not. The documents may come from teaching and research institutions in France or abroad, or from public or private research centers.

L'archive ouverte pluridisciplinaire **HAL**, est destinée au dépôt et à la diffusion de documents scientifiques de niveau recherche, publiés ou non, émanant des établissements d'enseignement et de recherche français ou étrangers, des laboratoires publics ou privés.

Public Domain

Thermodynamic and structural properties of lipid-photosensitizer conjugates mixed with phospholipids: impact on the formation and stability of nano-assemblies.

David Chapron^{1,4}, Jean-Philippe Michel^{1,4}, Philippe Fontaine², Jérémy Godard³, Frédérique Brégier,^{3,4} Vincent Sol^{3,4}, Véronique Rosilio^{1,4,*}

¹ Université Paris-Saclay, CNRS, Institut Galien Paris-Saclay, F-91400 Orsay, France.

² Synchrotron SOLEIL, L'Orme des Merisiers, Départementale 128, 91190 Saint-Aubin, France

³ Univ. Limoges, LABCis, UR 22722, F-87000, Limoges, France

⁴ CNRS, GDR 2025 HappyBio, F-45067 Orléans cedex 2, France

*To whom correspondence should be addressed

Full postal address of affiliations:

- Université Paris-Saclay, CNRS, Institut Galien Paris-Saclay, 17 avenue des Sciences, F-91400 Orsay, France.

veronique.rosilio@universite-paris-saclay.fr

david.chapron@universite-paris-saclay.fr

jean-philippe.michel@universite-paris-saclay.fr

- Synchrotron SOLEIL, L'Orme des Merisiers, Départementale 128, 91190 Saint-Aubin, France.

philippe.fontaine@synchrotron-soleil.fr

- Univ. Limoges, LABCis, UR 22722, 123 avenue Albert Thomas, F-87000, Limoges, France.

jeremy.godard@unilim.fr

frederique.bregier@unilim.fr

vincent.sol@unilim.fr

- CNRS, GDR 2025 HappyBio, Université d'Orléans, 14 rue d'Issoudun, BP 6744, 45067 Orléans cedex 2.

Abstract

The photosensitizer Phenalenone (PN) was grafted with one or two lipid (C_{18}) chains to form pure nano-assemblies or mixed lipid vesicles suitable for photodynamic therapy. Mixtures of PN- C_{18} conjugates with stearyl-oleoyl phosphatidylcholine (SOPC) form vesicles that disintegrate into bilayer sheets as the concentration of PN- C_{18} conjugates increases. We hypothesized that PN- C_{18} conjugates control the thermodynamic and structural properties of the mixtures and induce the disintegration of vesicles due to PN π - π -interactions.

Monolayers were analyzed by surface pressure and grazing incidence X-ray diffraction (GIXD) measurements, and vesicles by differential scanning calorimetry and cryo-TEM. The results showed that PN-triazole- C_{18} (**1A**) and PN-NH- C_{18} (**1B**) segregate from the phospholipid domains. PN- $(C_{18})_2$ (conjugate **2**) develops favorable interactions with SOPC and distearoyl-phosphatidylcholine (DSPC). GIXD demonstrates the contribution of SOPC to the structuring of conjugate **2** and the role of the major component in controlling the structural properties of DSPC-conjugate **2** mixtures. Above 10 mol% conjugate **2** in SOPC vesicles, the coexistence of domains with different molecule packing leads to conjugate segregation, vesicle deformation, and the formation of small bilayer discs stabilized by the inter-bilayer π - π stacking of PN molecules.

Keywords

Phenalenone ; phospholipid ; Langmuir monolayer ; vesicle ; grazing incidence X-ray diffraction ; DSC.

1. Introduction

Phenalenone (PN) is a natural photosensitizer (PS) well known for its ROS-mediated protective phytochemical activities¹ but also for its anticancer and antimicrobial photodynamic properties.²⁻⁴ To favor an application in antimicrobial photodynamic therapy (aPDT), a PS should be water soluble, be stable in solution, and have a high singlet oxygen quantum yield. PN is considered a universal reference molecule for singlet oxygen production, with a quantum yield close to unity in a large variety of solvents including water.^{5,6} Depending on the medium in which it is solubilized, PN may produce either ROS (reaction I) or singlet oxygen (reaction II), the latter reaction being favored in a hydrophobic environment.^{7,8} Whether it is solubilized in membranes or in the cytosol of targeted cells is thus of paramount importance for its therapeutic effectiveness. With a log P close to 3, PN is lipophilic⁹ and spontaneously aggregates in aqueous media.¹⁰ Its poor solubility makes it difficult to apply in therapeutics and can lower its singlet oxygen quantum yield by self-quenching effect at the excited state.^{11,12} PS efficiency is usually improved when incorporated into lipidic supramolecular assemblies such as micelles, oil-in-water emulsions, or lipid vesicles.^{11,13,14} Micelles and lipidic nanostructures allow to increase the concentration of the PS in aqueous media, without unwanted aggregation. The small size of these systems, especially micelles, seems advantageous for their efficacy.¹¹ However, phenalenone is difficult to insert in micelles and vesicle bilayers.

Previous works have shown that the conjugation of lipid chains with a hydrophilic or hydrophobic drug may lead to the formation of supramolecular assemblies, highly concentrated in the compound of interest.^{15,16} Nano-assemblies of lipid-drug conjugates can contain up to 50 mol% of a drug. They are often nanostructured, which may confer them greater stability and, in the case of lipid-PS conjugates, enhances their photosensitizing properties.^{17,18} The formation and stability of nano-assemblies made of lipid-PS conjugates

are dependent on the geometry and thermodynamic properties of the lipid-PS molecules.^{19,20} When these compounds cannot form pure nano-assemblies, they can be mixed at high molar ratios with other lipids like phospholipids or cholesterol to form vesicles.^{19,21}

One of the major difficulties when treating microbial infections is the destruction of the biofilms which consist of polymeric matrices protecting bacterial colonies against external conditions. These biofilms are an increasing cause of bacterial resistance against conventional antibiotics.²² It has been shown that lipidic nano-assemblies favor the permeation of photosensitizers into biofilms, helping them to diffuse inside the matrix and reach bacteria.^{23,24}

In recent work, two approaches were studied to modify phenalenone by lipid chains.¹⁰ Two conjugates with a stearic chain (PN-C₁₈, conjugates **1A** and **1B**) differing only in the nature of the linker to phenalenone (amide or amide + triazole), and PN-(C₁₈)₂ (conjugate **2**) in which PN is conjugated with two C₁₈ chains were synthesized. Conjugate **2**, whose chemical structure resembles that of a phospholipid proved able to self-assemble into large bilayer stacks at 40°C (Figure 1). When mixed with stearyl oleoyl phosphatidylcholine (SOPC) at molar fractions ranging from 10 to 40% at the same temperature, the three compounds **1A**, **1B**, and **2** formed vesicles. However, these vesicles were unstable over time. CryoTEM images showed heterogenous mixtures of small and oligolamellar vesicles, sheets, stacks of bilayers, and ribbon-like structures, all of which appeared to result from the destabilization of initially formed multilamellar vesicles.¹⁰

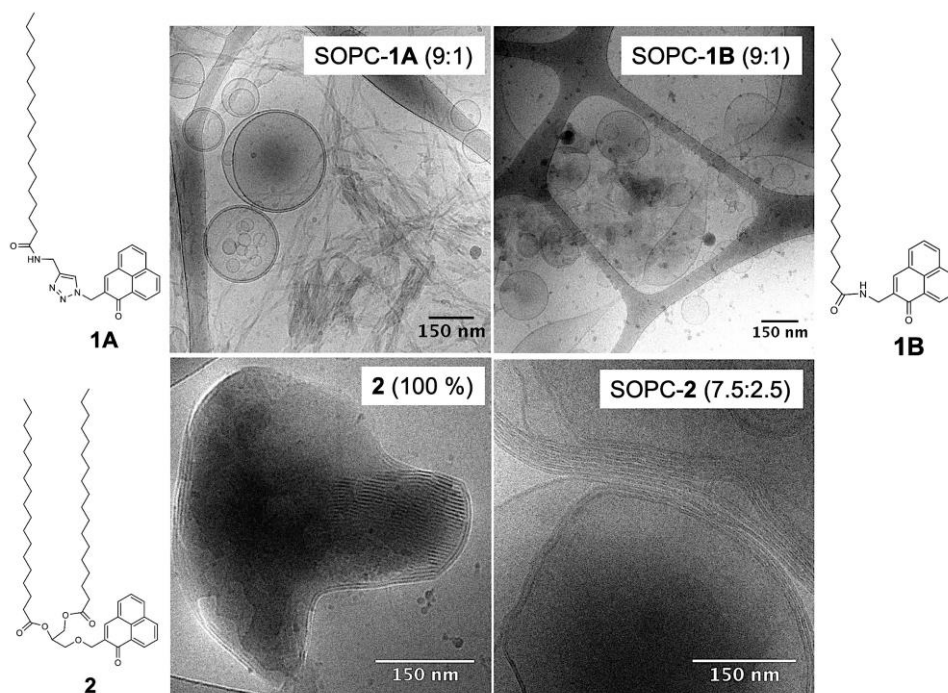


Figure 1: Chemical structure of compounds **1A**, **1B**, and **2**, and cryoTEM images of nano-assemblies obtained at 40°C with them and SOPC. CryoTEM conditions are described in ref 10.

To better understand the behavior of these conjugates in mixtures with phospholipids and identify the optimal conditions for the formation of stable nano-assemblies, like the temperature and lipid/PN derivative ratio, the nature of the linker or the number of lipid chains, we analyzed, in this work, the thermodynamic and structural properties of the three PN conjugates **1A**, **1B**, and **2** in mixtures with two phospholipids with the same chain length, SOPC (18:1) and distearoylphosphatidylcholine, DSPC (18:0).

2. Materials and methods

2.1. Materials

The phenalenone-lipid conjugates, namely N-((1-((1-oxo-1*H*-phenalen-2-yl)methyl)-1*H*-1,2,3-triazol-4-yl)methyl)stearamide (PN-triazole-C₁₈, compound **1A**, M_w = 556.8 g/mol), N-((1-oxo-1*H*-phenalen-2-yl)methyl)stearamide (PN-NH-C₁₈, compound **1B**, M_w = 475.7 g/mol)

and 3-((1oxo-1*H*-phenalen-2-yl)methoxy)propane-1,2-diyl distearate (PN-(C₁₈)₂, compound **2**, M_w = 817.3 g/mol) were synthesized as previously described.¹⁰ 1-Stearoyl-2-oleoyl-sn-glycero-3-phosphocholine (SOPC, M_w = 787.609 g/mol) and 1,2-distearoyl-sn-glycero-3-phosphocholine (DSPC, M_w = 789.625 g/mol) (Figure S1) were purchased from Avanti Polar Lipids, Inc., Alabaster, AL, USA. Chloroform and methanol used for the solutions in a ratio (9:1 v/v) were > 99.80% pure Carlo Erba reagents. Ultrapure milliQ water was produced by a Millipore Milli-Q® Direct 8 Water Purification System.

2.2. Methods

2.2.1. *Thermal analysis of hydrated phospholipid-phenalenone conjugates mixtures*

Thermal analysis was carried out using a MicroCal VP-DSC instrument (Northampton, MA, USA) at 1°C/min scan rate between 1°C and 60°C under approximately 25 psi positive cell pressure. Phospholipid-PN-C₁₈ mixtures (2 mM) were dissolved in a mixture of chloroform and methanol (9:1, v/v) and the solvents were evaporated under reduced pressure. The film obtained was hydrated by pure water at 60°C, and the resulting lipid suspension was vortexed for few minutes with glass beads until the film was detached from the flask wall.

Prior to the analysis of each lipid mixture and after cell cleaning, one heating was performed with pure water in the sample and reference cells. Three heating/cooling cycles were then recorded for each sample. The feedback mode/gain was set on high. Thermograms were analyzed using the Trios software (version 4.4) and enthalpy variations (ΔH) were calculated by integrating the area under transition peaks.

Pure conjugate **2** was also analyzed using a DSC Diamond calorimeter (PerkinElmer) calibrated with Zinc and Indium. Three heating/cooling cycles were performed between 20

and 75°C, at 5°C/min. A solution of conjugate **2** in chloroform and methanol (9:1, v/v) was deposited into a 50 µl DSC pan and evaporated overnight under reduced pressure to form a film covering the bottom of the pan. The sample was accurately weighted (1.10 ± 0.5 mg) and 15 µl of water were added before the pan was sealed. Several heating/cooling cycles were then performed between 25 °C and 75 °C until heating scans were reproducible.

2.2.2. Surface pressure measurements

Surface pressure-surface area (π -A) measurements were performed using a thermostated Langmuir film trough (775.75 cm², Biolin Scientific, Finland) enclosed in a plexiglas box, protected from light. All experiments were performed at 22 ± 1 °C. After spreading, each system was left for 15 min to allow complete evaporation of the organic solvents. Monolayer compression was performed at $6 \text{ \AA}^2 \cdot \text{molecule}^{-1} \cdot \text{min}^{-1}$ speed. Results are mean values of at least 3 measurements. The experimental uncertainty was estimated to be 0.2 mN/m. The surface compressional moduli (C_s^{-1}) of monolayers were calculated from the equation (1):

$$C_s^{-1} = -A \frac{d\pi}{dA} \quad (1)$$

The free energy of mixing is the sum of the excess free energy and the ideal free energy calculated using equations (2) and (3):

$$\Delta G^{exc} = \int_0^\pi (A_{mix} - x_1 A_1 - x_2 A_2) d\pi \quad (2)$$

$$\Delta G^{ideal} = nRT(x_1 \ln x_1 + x_2 \ln x_2) \quad (3)$$

With A_{mix} , the experimental molecular area for the mixture at a given surface pressure, A_1 and A_2 , the molecular area of the pure components at the same surface pressure and x_1 , and x_2 , the molar fraction of each component in the mixture.²⁵

2.2.3. GIXD measurements under synchrotron radiation

X-ray diffraction measurements were taken on the SIRIUS beamline at the SOLEIL Synchrotron (Saint Aubin, France).²⁶ The incident X-ray energy was 8 keV ($\lambda = 1.55 \text{ \AA}$), and the beam size was $0.1 \times 1 \text{ mm}^2$. Grazing incidence X-ray diffraction (GIXD) was performed on monolayers, made of conjugate **2**, pure or mixed with a phospholipid, to obtain in-plane and out-of-plane information about the molecular ordering at the air/water interface. Monolayers were spread on the water subphase of a custom-built Langmuir trough enclosed in a temperature-controlled sealed chamber (21°C) and flushed with helium during data collection to reduce the gas scattering and avoid beam damage to the monolayer. After spreading, the lipid film was left for 15 minutes to allow for solvent evaporation and film relaxation, and then compressed at $3 \text{ \AA}^2 \cdot \text{molec}^{-1} \cdot \text{min}^{-1}$. The water surface was illuminated at an incident angle of 2.0 mrad below the critical angle of the air-water interface (2.8 mrad at 8 keV), so that the incident wave was totally reflected, while the refracted wave became evanescent, exploring a layer several nanometers deep beneath the interface. The diffraction pattern was collected using a Pilatus3 detector (Dectris, Switzerland) associated with a Soller slit collimator (JJ-Xray, Denmark, resolution 0.06 deg) by scanning in the in-plane angle 2θ . Q_{xy} - Q_z images were generated by integrating horizontally the window defined by the Soller slit collimator on the original raw 2-D file of the detector to obtain the vertical distribution of the intensity. Further information on data processing is provided in the Supporting Information.

2.2.4. Formation and characterization of phospholipid-phenalenone conjugate nano-assemblies.

Pure conjugates **1A**, **1B**, or **2** and SOPC were dissolved in a mixture of chloroform and methanol (9:1, v/v) and the solvents were evaporated under reduced pressure to remove all residual solvents. The resulting film was hydrated by pure water at 40°C for conjugates **1A**

and **1B**, and at 65°C for conjugate **2**. The obtained lipid suspension was sonicated twice for 5 min by a series of 10 s-on/10 s-off cycles using a Branson SFX150 probe sonicator (150 W, 40 kHz, Branson Ultrasonics™, Emerson) at 20% amplitude. Suspensions obtained with pure conjugate **2** were used without further processing. Formulations containing mixtures of SOPC and the conjugates were centrifuged at 3000g for 15 min. All obtained nano-assembly suspensions were stored under nitrogen at 4°C in the dark. Dynamic light scattering (DLS) and zeta potential measurements were carried out in triplicate at 25°C, using a Zetasizer Nano-ZS 90 (Malvern Instruments Ltd, UK). The morphology of the nano-assemblies was analyzed using a ThermoFischer Scientific G3 Titan Themis 300 transmission electron microscope equipped with a Cryo-Box anticontamination system and a C-Twin objective lens (Cs = 2.7 mm, Cc = 2.7 mm, Focal length = 3.5 mm), using accelerating voltage of 300 kV, with the following illumination conditions: spot size of 5, a 150 µm condenser aperture, and no objective aperture. Images were recorded (defocus range: -0.3 to 0.4 µm) using the low electron dose system (10 e⁻/Å² per sec), with a magnification of 5,400x and 58,000x on a ThermoFischer Scientific™ Falcon 3 EC Direct Detection Electron 4Kx4K camera in linear mode. 4 µL of each suspension were deposited on a 300-mesh lacey carbon-coated grid. After removal of the excess liquid with a filter paper, the grid was quickly frozen in liquid ethane and inserted in the microscope using a nitrogen-cooled side entry Gatan Elsa™ (698) Cryo-holder at -181°C.²⁷

3. Results

3.1. Thermodynamic properties of mixtures of phospholipid and phenalenone-lipid conjugates

3.1.1. *Conjugates 1A and 1B*

The thermograms for hydrated conjugate **1A-SOPC** and conjugate **1B-SOPC** mixtures are shown in Figure 2, and the corresponding phase transition temperatures and enthalpies are presented in Table S1 and Figures S2 and S3. In the studied temperature range, conjugates **1A** and **1B** do not display any specific thermal properties. SOPC exhibits a phase transition temperature at 5.4°C, without any pretransition, in agreement with the literature.²⁸ This phase transition temperature slightly decreases as the molar fraction of compound **1A** increases, and the enthalpies are gradually reduced from 5.3 to 0.6 kcal/mol lipid for the pure SOPC and the mixture containing 65 mol% conjugate **1A**, respectively. Above 65 mol% **1A**, the phase transition peak of SOPC completely disappears. Conjugate **1B** also affects the thermal behavior of SOPC, with a weak increase of the phase transition temperature of the phospholipid with the molar fraction of conjugate **1B** (Figure 2b, Table S1, Figure S3). The enthalpy peak of SOPC is enlarged up to 50 mol% **1B**, then gradually fades and virtually disappears at 70 mol% **1B**.

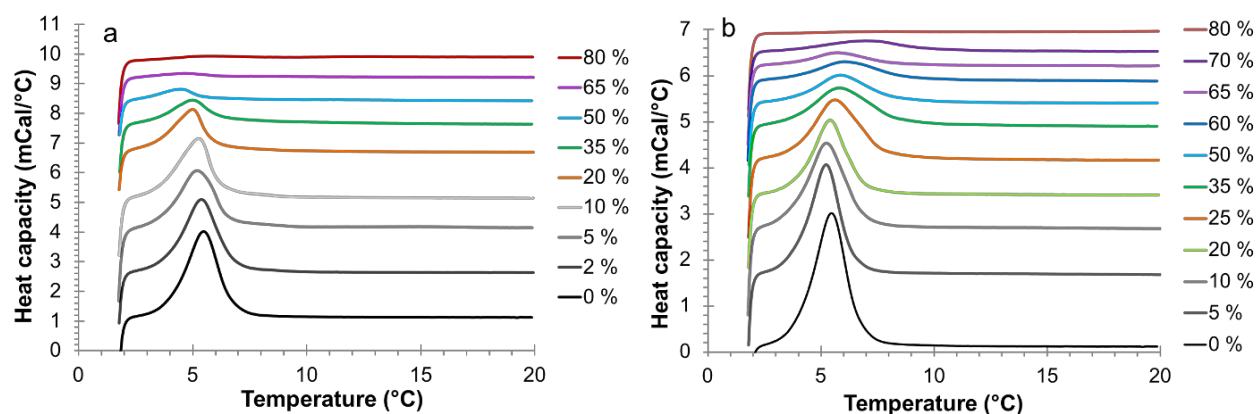


Figure 2: Thermograms of SOPC mixtures with compounds **1A** (a) and **1B** (b) with increasing mol% of the conjugates.

Surface pressure vs. molecular area isotherms for monolayers of SOPC mixed with the two PN conjugates show that compounds **1A** and **1B** alter the interfacial behavior of the

phospholipid, however in a different manner (Figures S4 and S5). Conjugate **1A** tends to increase the compressibility of SOPC monolayers, whereas conjugate **1B** rigidifies them. Excess free energies are positive at all SOPC-**1A** ratios and all surface pressures while for conjugate **1B**, positive and negative excess free energies are obtained depending on the molar fraction of the compound (Figure 3 and Tables S2 and S3). SOPC mixes better with **1B** than with **1A**.

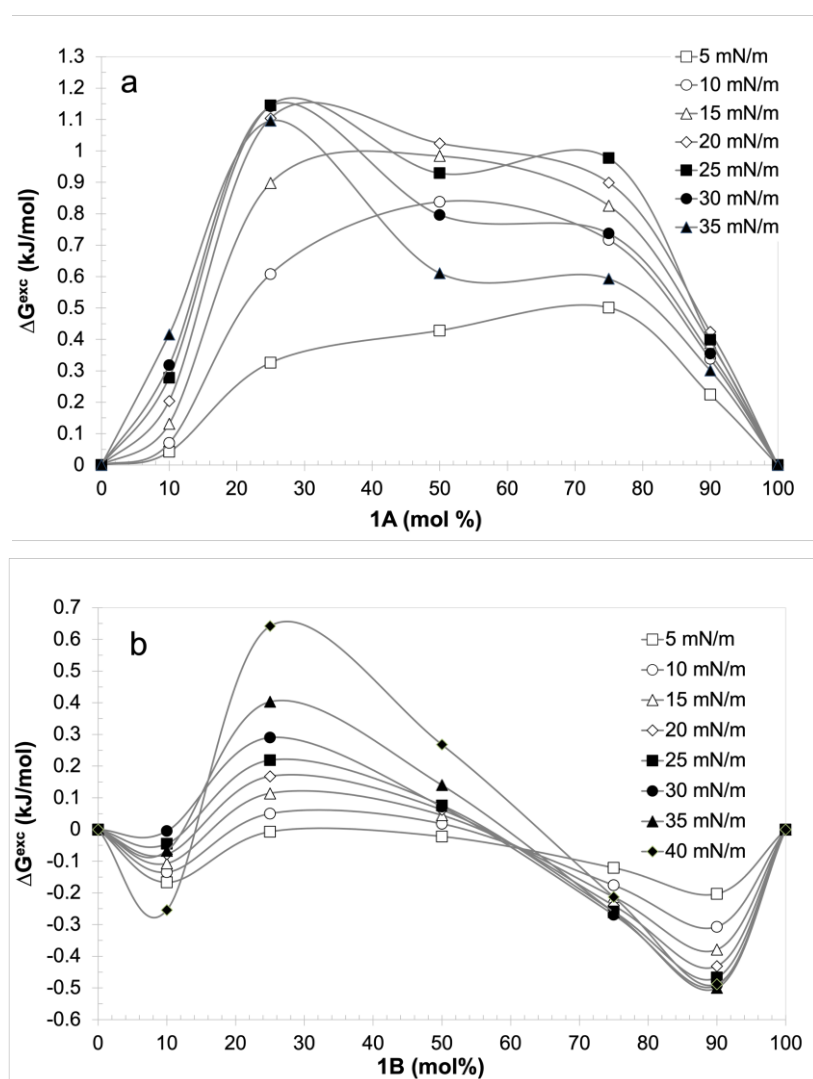


Figure 3: ΔG^{exc} values versus the molar fraction of the phenalenone-lipid conjugate for (a) for **1A**-SOPC and (b) **1B**-SOPC mixtures.

3.1.2. Conjugate 2

Pure conjugate **2** exhibits a phase transition temperature at 47°C (T_{m2}). At high SOPC molar fractions, the observed transition is shifted to a slightly higher temperature, around 48°C (Figure 4a, Table S4). The peak is thinner, and better defined than at the highest concentrations of the PN derivative. Like conjugates **1A** and **1B**, conjugate **2** affects the thermal behavior of SOPC: an increase in the phase transition temperature and gradual lowering of the enthalpies values for the phospholipid are observed as the molar ratio of the conjugate increases (Figure 4a and Figure S6). Although the deviation of experimental enthalpy data from theoretical ones is small, there is evidence that conjugate **2** penetrates and disorganizes the SOPC domains. Above 50 mol% of conjugate **2**, the phase transition peak of SOPC (T_{m1}) is no longer visible. From 5 to 50 mol% of conjugate **2**, both peaks appear on the thermograms, suggesting a phase separation, with the coexistence of conjugate **2**-SOPC mixed domains and quasi-pure conjugate **2** domains (very thin peaks).

To analyze the effect of a phospholipid bearing more resemblance to conjugate **2**, DSC measurements were also performed with the saturated distearoylphosphatidylcholine (DSPC) (Figure 4b, Table S4, and Figure S7). DSPC, like conjugate **2**, forms structured gel phase mono- and bilayers at 22°C and rigid monolayers. The thermograms of the fully hydrated DSPC bilayers exhibit a weak peak at 49.3°C assigned to the $L\beta'$ gel phase \rightarrow $P\beta'$ ripple phase pretransition and a sharp peak at 54°C (T_{m3}) corresponding to the $P\beta' \rightarrow L\alpha$ transition (lamellar liquid crystalline phase), in agreement with the literature.²⁹ At 5 mol% of conjugate **2** and above, the pre-transition of DSPC vanishes. At 20 mol% of conjugate **2**, the phase transition peak of the conjugate appears (T_{m2}) indicating a phase separation.

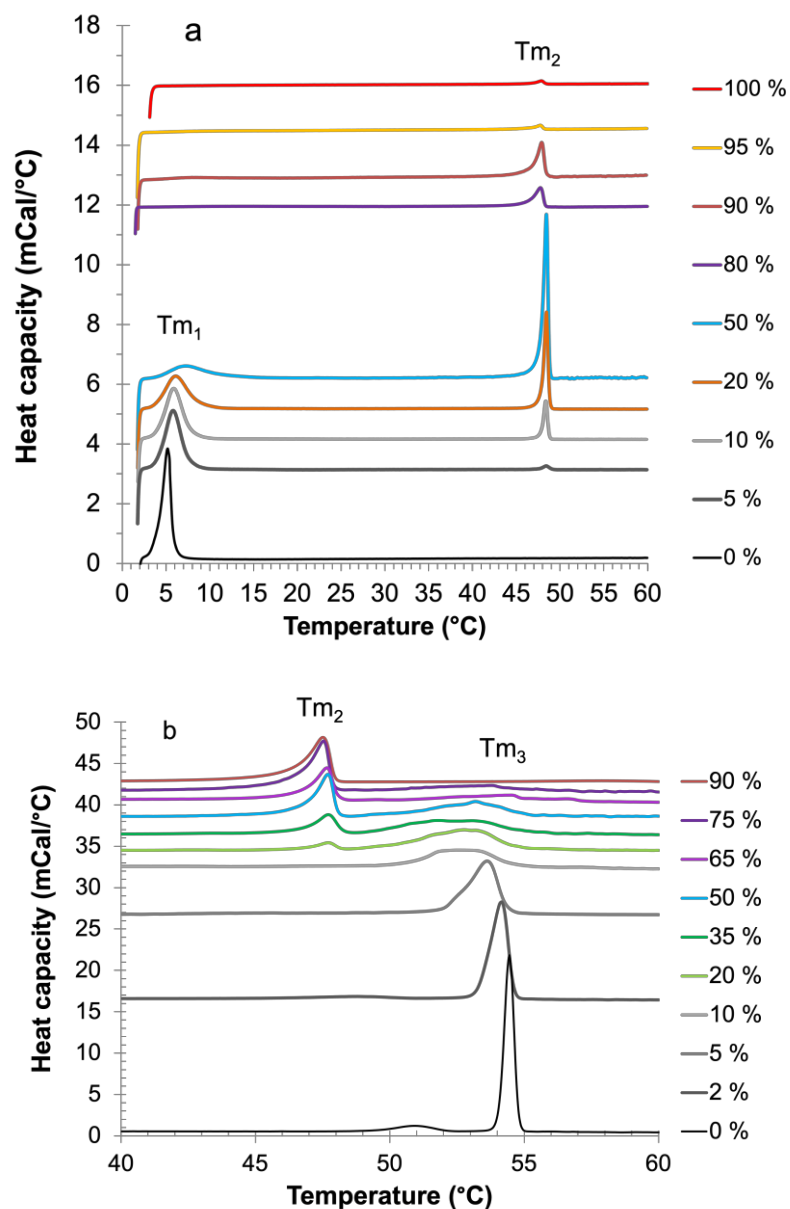


Figure 4: Thermograms of (a) conjugate **2**-SOPC and (b) conjugate **2**-DSPC mixtures. T_{m1} , T_{m2} and T_{m3} are the phase transition temperatures of SOPC, conjugate **2**, and DSPC, respectively. In (a) the decrease in the enthalpy of conjugate **2** at high molar fractions corresponds to a loss of material due to the impossibility to remove completely the film of the conjugate from the vial after rehydration.

When spread at the air/water interface, conjugate **2** forms rigid monolayers (Figure 5 and Figure S8). Compared to pure SOPC and DSPC monolayers,^{30,31} monolayers of conjugate **2** exhibit a smaller molecular area and higher surface pressure at collapse. The profiles of the isotherms for the mixtures suggest an interaction between the conjugate and the two phospholipids. This interaction, favorable, is confirmed by the negative values of the calculated excess free energies (Figure 6, Tables S5 and S6). Contrarily to conjugates **1A** and **1B**, Conjugate **2** forms stable mixtures with the two studied phospholipids at all molar fractions and surface pressures.

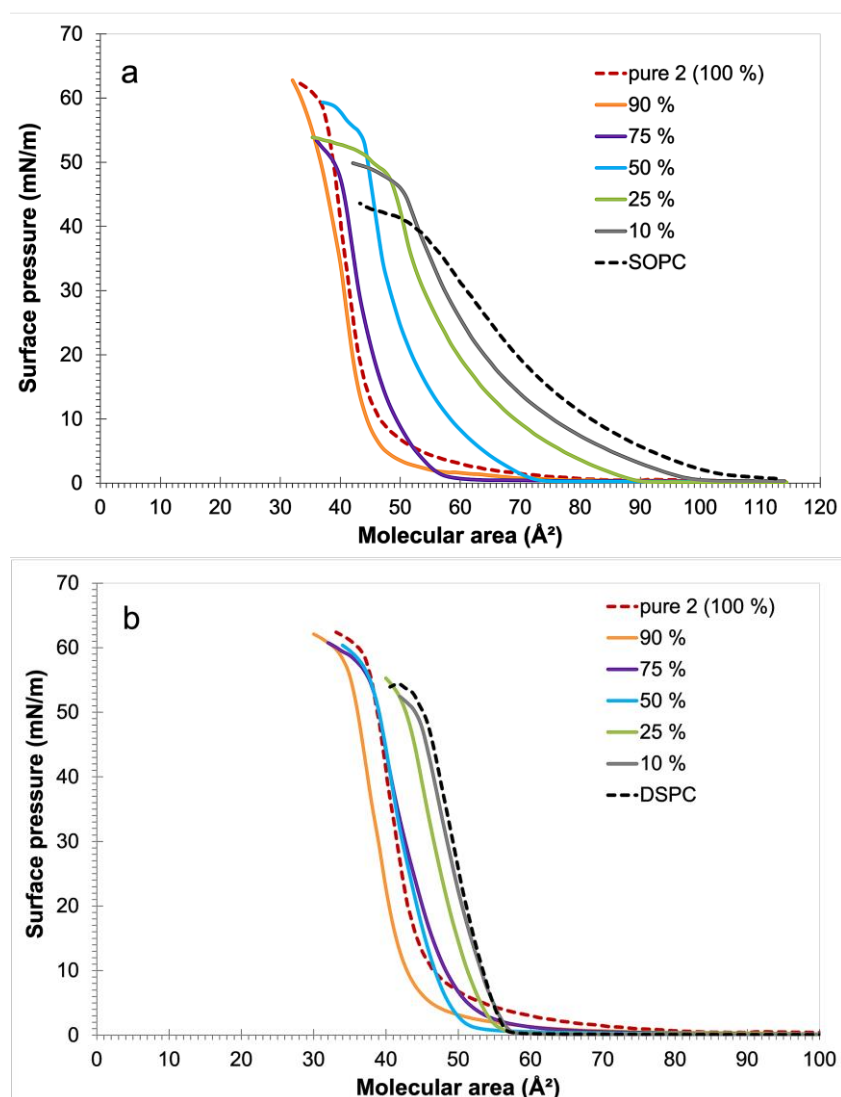


Figure 5: π -A isotherms for (a) **2**-SOPC and (b) **2**-DSPC mixed monolayers.

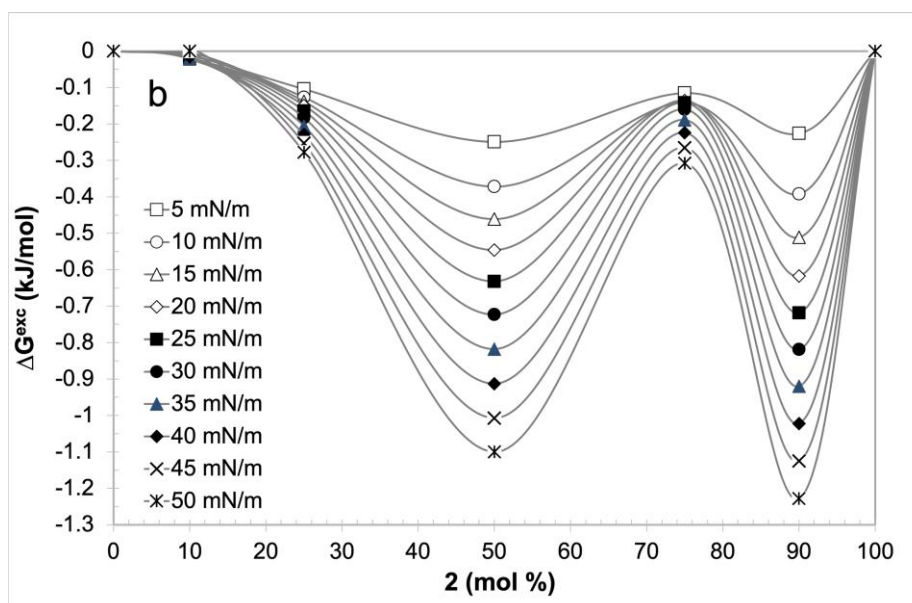
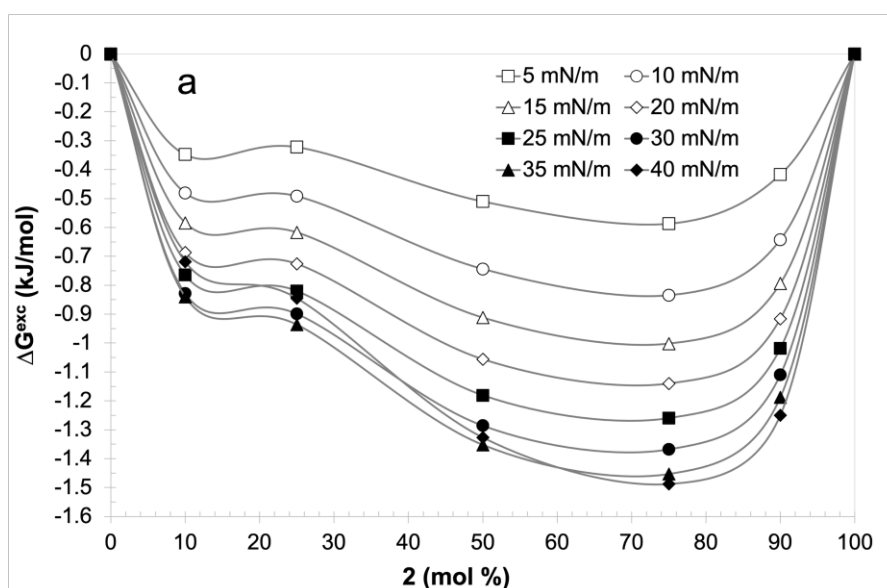


Figure 6: ΔG^{exc} values versus the molar fraction of the PN conjugate for mixtures of conjugate **2** with (a) SOPC and (b) DSPC, spread at air-water interface.

3.2. Structure of the mixed monolayers of conjugate **2** and phospholipids

To get a better insight into the structure of the mixtures of conjugate **2** with SOPC and DSPC, GIXD measurements were performed on monolayers of pure conjugate **2** as well as mixtures of conjugate **2** with both phospholipids. The pure SOPC monolayer does not diffract X-rays

whereas GIXD spectra for the pure DSPC monolayer exhibit one in-plane and one out-of-plane peaks at surface pressures higher than $5 \text{ mN}\cdot\text{m}^{-1}$ when the layer is in a Liquid Condensed phase.³²⁻³⁴ DSPC diffraction pattern could be indexed using the rectangular centered lattice with NN orientation and significant chain tilt from 30° at low surface pressure to 26° at $30 \text{ mN}\cdot\text{m}^{-1}$ (Table 1).

Monolayers of the pure conjugate **2** could diffract at all surface pressures studied, even at $0 \text{ mN}/\text{m}$ (Table 1, Table S7, Figure S9). As the surface pressure increases, the cell parameters, as deduced from the position of the peaks, evolve from a rectangular structure to pure hexagonal packing. The full width at half maximum of the in-plane Bragg peaks is almost stable with surface pressures and corresponds to in-plane correlation lengths of 16 nm on average, indicating an ordering which extends up to the second nearest neighboring molecules.

Compound **2** forms structured mixed monolayers with both SOPC and DSPC. Conjugate **2**-SOPC monolayers exhibit a pure hexagonal cell ($a/b = \sqrt{3}$) with chains in an upright position ($t = 0^\circ$) (Table 1 and Figure S10). When DSPC and conjugate **2** are mixed, an intense in-plane peak with a weak out-of-plane component is observed at all surface pressures (Figure S10, Table S7). All diffraction peaks can be indexed in the centered rectangular lattice with NN orientation. At a low conjugate **2** molar ratio ($10 \text{ mol}\%$), the structural parameters of the mixed monolayer are very close to those of pure DSPC. At higher conjugate **2** molar ratios (20 and $50 \text{ mol}\%$), the lattice symmetry evolves from a rectangular to a more hexagonal one as the surface pressure increases in the film. For DSPC-conjugate **2** mixtures, GIXD measurements demonstrate the predominance of the major component in the mixture on the structural properties of the mixed monolayer.

Table 1: Characteristic GIXD parameters for monolayers of conjugate **2** mixed with DSPC or SOPC. *Below 15 mN/m. R: rectangular. H: hexagonal. NN: Nearest neighbor. L_{xy} : correlation length.

System	π (mN/m)	0	5	15	30	40	Lattice Tilt- Orientation
Conjugate 2	A (\AA^2)	77.0	50.0	44.5	41.5	38.7	
	a/b (\AA)	4.89/8.35	4.86/8.33	4.77/8.27	4.87/8.25	4.84/8.25	R
	Tilt ($^\circ$)	7.9	5.8	0	0	0	NN*
	L_{xy} (nm)	15.3	17.2	22.4	11.6	13.7	
DSPC	A (\AA^2)	77.7	51.0	49.0	46.3	-	
	a/b (\AA)	-	5.53/8.64	5.36/8.58	5.26/8.58	-	R
	Tilt ($^\circ$)	-	>30	29.8	26.2	-	NN
	L_{xy} (nm)	-	20.6	15.1	23.9	-	
2 -DSPC 50 mol% 2	A (\AA^2)	77.2	50.5	47.6	44.6	-	
	a/b (\AA)	5.05/8.5	5.05/8.48	4.97/8.43	4.99/8.4	-	R
	Tilt ($^\circ$)	23.8	19.7	15.8	14.9	-	NN
	L_{xy} (nm)	13.7	12.5	12.9	10.1	-	
2 -DSPC 20 mol% 2	A (\AA^2)	77.2	54.0	51.6	48.7	46.8	
	a/b (\AA)	-	5.53/8.62	5.25/8.56	5.13/8.53	4.99/8.47	R
	Tilt ($^\circ$)	-	32.8	26.5	23.4	18.5	NN
	L_{xy} (nm)	-	19.3	13.0	18.1	16.2	
2 -DSPC 10 mol% 2	A (\AA^2)	77.0	54.7	52.5	49.6	48	
	a/b (\AA)	-	5.63/8.64	5.28/8.59	4.88/8.88	5.13/8.52	R
	Tilt ($^\circ$)	-	35.3	29.3	24	23	NN
	L_{xy} (nm)	-	27.4	21.9	22.0	18.8	
2 -SOPC 80 mol% 2	A (\AA^2)	96.0	54.0	48.7	44.9	42.9	H
	a/b (\AA)	-	4.81/8.33	4.79/8.29	4.77/8.26	4.76/8.25	
	Tilt ($^\circ$)	-	0	0	0	0	
	L_{xy} (nm)	-	10.9	12.7	13.9	11.0	
2 -SOPC 60 mol% 2	A (\AA^2)	96.5	61	53.6	48.3	46.0	H
	a/b (\AA)	-	4.8/8.32	4.78/8.28	4.77/8.27	4.77/8.26	
	Tilt ($^\circ$)	-	0	0	0	0	
	L_{xy} (nm)	-	12.7	14.5	17.0	14.9	
2 -SOPC 50 mol% 2	A (\AA^2)	96.5	72.0	63.3	56.0	52.7	H
	a/b (\AA)	4.83/8.37	4.81/8.34	4.79/8.3	4.78/8.29	4.78/8.29	
	Tilt ($^\circ$)	0	0	0	0	0	
	L_{xy} (nm)	11.75	9.5	12.6	14.1	13.1	
2 -SOPC 20 mol% 2	A (\AA^2)	96.8	82.0	68.4	59.0	55.0	H then R
	a/b (\AA)	4.81/8.33	4.78/8.29	4.77/8.26	4.76/8.26	4.84/8.24	
	Tilt ($^\circ$)	0	0	0	0	0	
	L_{xy} (nm)	20.2	22.4	21.0	17.1	28.9	

3.3. Formation of nano-assemblies of conjugate **2** with SOPC

Considering the high phase transition temperature of the PN derivative, nano-assemblies were formed with pure conjugate **2** and SOPC at 65°C instead of 40°C in the previous study. A clear evolution of the morphology of the nano-assemblies was observed depending on the content in conjugate **2**. At 10 mol% of conjugate **2**, small unilamellar (SUVs) and multilamellar vesicles (MLVs) were formed (Figure 7). The DLS report showed significant polydispersity with three peaks at 141.4 ± 23.9 , 537.9 ± 65.2 , and 44.2 ± 4.7 nm (55.3%, 24.9%, and 19.8% intensity, respectively). The zeta potential values were negative (about -5 mV for pure SOPC and -20 mV for pure conjugate **2**). At 25 mol% and above, nanoobjects with different morphologies were observed like faceted SUVs or stacked bilayers. At 75 mol% of conjugate **2**, however, deformed MLVs and stacked bilayers appeared predominant.

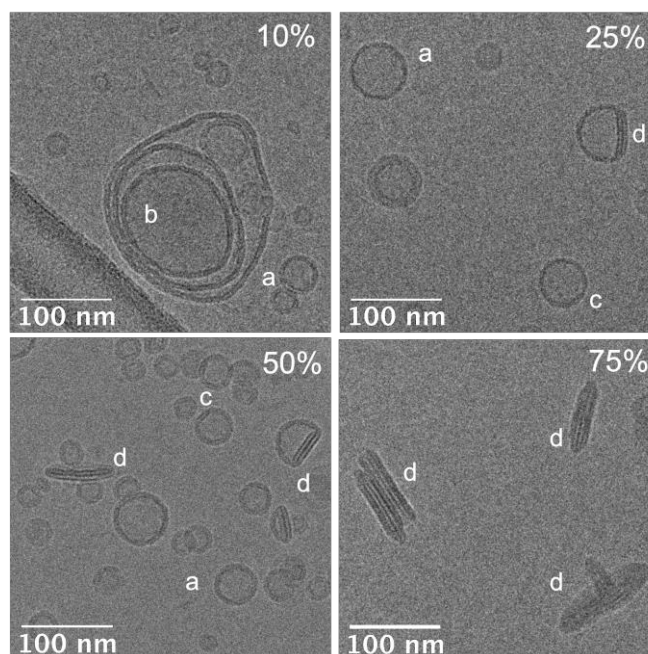


Figure 7: CryoTEM images showing the morphology of conjugate **2**-SOPC nano-assemblies obtained at 65°C and containing 10 to 75 mol% of conjugate **2**. a: SUV, b: MLV, c: faceted SUV, d: stacked bilayers.

4. Discussion

The formation of nano-assemblies of phenalenone-lipid conjugates with single or double C₁₈ chains is not straightforward. Conjugates **1A** and **1B** cannot form micelles. We have shown previously that when mixed with SOPC they formed unstable vesicles which transformed into bilayer sheets and ribbons.¹⁰ In this work, DSC and surface pressure measurements demonstrate that conjugates **1A** and **1B** affect SOPC thermodynamic properties and tend to segregate. This segregation can be partially explained by the unfavorable interaction observed by other authors between the stearic acid chain and an unsaturated phospholipid like DOPC,³⁵ but not only. The conjugate **1A** is clearly more disruptive to monolayers and bilayers than the conjugate **1B**. Apparently, this disruption results more from the bulkiness of the conjugate **1A** linker and the complex interactions developed in the plane of the interface, than from hydrophobic interactions between the C₁₈ chains. Indeed, in addition to π - π interactions between PN molecules, the amide and triazole groups may form hydrogen bonds with water and neighbor molecules which would rigidify the molecules and contribute to phase separation. According to Doiron *et al.*³⁶, a triazole group influences the shape of a molecule and makes it less planar than when the linker is an amide group. The amide group is a stronger hydrogen bond donor and acceptor than the triazole. It promotes intramolecular H-bonds that are lost with the triazole cycle. The triazole also weakens intermolecular hydrogen bonds. For conjugate **1A**, whose linker contains both groups, interactions with neighboring molecules could be particularly complex at the level of the polar head region.

For conjugate **2**, DSC and GIXD results suggest that instead of solubilizing the PN derivative, SOPC has a structuring effect on its domains. The phospholipid molecules increase the

symmetry of the cell and participate in the structuring of conjugate **2** domains, preserving the extent of the 2D order of these domains. Monolayers are rigidified above 25-30 mN/m, a surface pressure considered as mimicking the lateral pressure in bilayers.³⁷

The disappearance of the pre-transition of DSPC in thermograms of its mixtures with conjugate **2** indicates that PN moieties interact with the phospholipid headgroups. They are thus likely to be partially immersed in the water phase.

The double interaction of conjugate **2** with the phospholipids, at the level of the polar heads and at the level of the hydrophobic chains has a strong influence on the formation and stability of liposomes. Below 20 mol%, the effect of conjugate **2** is limited. This explains that multilamellar and unilamellar vesicles are predominant in the sample with 10% conjugate **2**. However, at 20 mol% and above, molecules of conjugate **2** get closer and strongly interact with one another, forming rigid domains. It is well known that when liquid-crystalline and gel phases coexist in a bilayer, the molecules at the domain boundaries have different packing.³⁸ Molecules of conjugate **2** in the gel phase are more tightly packed than those of SOPC in the liquid-crystalline phase. The polyhedral (faceted) morphology of vesicles results from the existence of these lipid domains with different molecule packing and orientation, and defects at domain boundaries.³⁹ The increase in bilayer curvature leads to the reduction in the size of liposomes, breaking of vesicles, and formation of small bilayer discs with two or more stacked bilayers.

The formation of planar bilayers is generally associated with a difference in the packing parameter of the vesicle-forming components. This may be the case for conjugate **1A** and **1B** which must have a lower packing parameter than the phospholipid, but this is less expected from conjugate **2** which packing parameter is probably close to that of SOPC. For the three conjugates, it seems that the inter-bilayer stacking of PN molecules would be ultimately responsible for the disintegration of vesicles. CryoTEM images show that vesicles adhere to

each other and to bilayer discs. A similar bridging phenomenon based on polar head interactions between liposome bilayers has been described for aescin-containing liposomes.⁴⁰

The increase in conjugate **2** concentration up to 75 mol% enhances this phenomenon and leads to small discs forming (about 100 nm in diameter).

5. Conclusion

Phenalenone-lipid conjugates have been synthesized with the objective to form pure nano-assemblies or mixed vesicles with SOPC containing a high concentration of PN, for its use in aPDT. However, when pure, these derivatives either do not self-assemble (conjugates **1A** and **1B**) or form large cohesive bilayer stacks (conjugate **2**). When mixed with SOPC, conjugates **1A** and **1B** form multilamellar vesicles that rapidly disintegrate into large bilayer sheets and ribbons. Interestingly, conjugate **2** above 10 mol% leads to the formation of altered vesicles that evolve into small bilayer discs predominating at 75 mol%. The destabilization of vesicles and formation of multi-bilayer discs result from phospholipid-conjugate segregation in bilayers and lateral and inter-bilayer π - π interactions of phenalenone heads. The stability over time of these discs remains to be assessed, before testing the antimicrobial efficacy of these small bilayer discs on bacteria strains and their biofilms.

CRedit authorship contribution statement

DC: Methodology, Investigation, Validation; **JPM:** Investigation, Formal analysis; **PF:** Methodology, Validation; **JG:** Resources; **FB:** Resources; **VS:** Resources, Supervision; **VR:** Conceptualization, Methodology, Validation, Supervision, Writing, Review & Editing.

Declaration of Competing Interest

The authors declare that they have no known competing financial interests or personal relationships that could have appeared to influence the work reported in this paper.

Data Availability

The data presented in this study are available on request from the corresponding author.

Acknowledgments

The authors would like to acknowledge SOLEIL for the provision of synchrotron radiation facilities and the use of SIRIUS Beamline in projects 20200096 and 20210232. They also thank the CIMEX – Ecole Polytechnique, IP Paris, Palaiseau Cedex, France, and Dr. Eric Larquet for cryoTEM images and helpful discussions. This research was funded by CNRS.

Appendix A. Supporting information

References

1. Song R, Feng Y., Wang D., Xu Z., Li Z., Shao X., Phytoalexin phenalenone derivatives inactivate mosquito larvae and root-knot nematode as type-II photosensitizer, *Sci. Rep.* 7 (2017) 42058. <https://doi.org/10.1038/srep42058>.
2. Späth A., Leibl C., Cieplik F., Lehner K., Regensburger J., Hiller K.-A., Bäumler W., Schmalz G., Maisch T., Improving photodynamic inactivation of bacteria in dentistry: highly effective and fast killing of oral key pathogens with novel tooth-colored type-II photosensitizers, *J. Med. Chem.*, 57 (2014) 5157-5168. <https://dxdoi.org/10.1021/jm4019492>.
3. Salmeron M.L., Quintana-Aguilar J., De La Rosa J.V., Lopez-blanco F., Castrillo A., Gallardo G., Tabraue C., Phenalenone-photodynamic therapy induces apoptosis on

- human tumor cells mediated by caspase-8 and P38-MAPK activation, *Mol. Carcinog.* 57 (2018) 1525-1539. <https://doi.org/10.1002/mc.22875>.
4. Kaye E.G., Kailass K., Sadovski O., Beharry A.A., A green-absorbing, red-fluorescent phenalenone-based photosensitizer as a theranostic agent for photodynamic therapy, *ACS Med. Chem. Lett.* 12 (2021) 1295-1301. <https://doi.org/10.1021/acsmchemlett.1c00284>
 5. Schmidt R., Tanielian C., Dunsbach R., Wolff C., Phenalenone, a universal reference compound for the determination of quantum yields of singlet oxygen $O_2(^1\Delta_g)$ sensitization, *J. Photochem. Photobiol. A: Chem.* 79 (1994) 11-17. [https://doi.org/10.1016/1010-6030\(93\)03746-4](https://doi.org/10.1016/1010-6030(93)03746-4)
 6. Segado M., Reguero M., Mechanism of the photochemical process of singlet oxygen production by phenalenone, *Phys. Chem. Chem. Phys.* 13 (2011) 4138-4148. <https://doi.org/10.1039/c0cp01827a>
 7. Lorente C., Arzoumanian E., Castano C., Oliveros E., Thomas A.H., A non-singlet oxygen mediated reaction photoinduced by phenalenone, a universal reference for singlet oxygen sensitization, *RSC. Adv.* 2014, 4, 10718-10727. <https://doi.org/10.1039/c3ra46867d>
 8. Espinoza C., Trigos A., Medina M.E., Theoretical study on the photosensitizer mechanism of phenalenone in aqueous and lipid media, *J. Phys. Chem. A.*, 120 (2016) 6103-6110. <https://doi.org/10.1021/acs.jpca.6b03615>
 9. Freijo M.B., Lopez-Arencibia A., Pinero J.E., McNaughton-Smith G., Abad-Grillo T., Design, synthesis and evaluation of amino-substituted 1*H*-phenalen-1-ones as anti-leishmanial agents, *Eur. J. Med. Chem.* 143 (2018) 1312-1324. <https://doi.org/10.1016/j.ejmech.2017.10.032>

10. Godard J., Chapron D., Bregier F., Rosilio V., Sol V., Synthesis and supramolecular arrangement of new stearyl acid-based phenalenone derivatives, *Colloids Surf. A: Physicochem. Engineer. Asp.* 612 (2021) 125988. <https://doi.org/10.1016/j.colsurfa.2020.125988>
11. Tsai T., Yang Y.-T., Wang T.-H., Chien H.-F., Improved photodynamic inactivation of gram-positive bacteria using hematoporphyrin encapsulated in liposomes and micelles, *Lasers Surg. Med.* 41 (2009) 316-322. <https://doi.org/10.1002/lsm.20754>
12. Pereira L.S.A., Camacho S.A., Almeida A.M. Jr, Gonçalves R.S., Caetano W., DeWolf C., Aoki P.H.B., Mechanism of hypericin incorporation to explain the photooxidation outcomes of phospholipid biomembrane models, *Chem. Phys. Lipids*, 244 (2022) 105181. <https://doi.org/10.1016/j.chemphyslip.2022.105181>
13. Boyle R.W., Dolphin D., Structure and biodistribution relationships of photodynamic sensitizers, *Photochem. Photobiol.* 64 (1996) 469-485. <https://doi.org/10.1111/j.1751-1097.1996.tb03093.x>
14. Chen C.-T., Chen C.-P., Yang J.-C., Tsai T., Liposome-encapsulated photosensitizers against bacteria, *Recent Pat. Antiinfect. Drug Discov.* 8 (2013) 100-107. <https://doi.org/10.2174/1574891x113089990011>
15. Lepeltier E., Bourgaux C., Rosilio V., Poupaert J.H. Meneau F., Zouhiri F., Lepêtre-Moulhi S., Desmaële D., Couvreur P., Self-assembly of squalene-based nucleolipids: relating the chemical structure of the bioconjugates to the architecture of the nanoparticles, *Langmuir* 29 (2013) 14795-14803. <https://doi.org/10.1021/la403338y>
16. Lepeltier E., Bourgaux C., Maksimenko A., Meneau F., Rosilio V., Sliwinski E., Zouhiri F., Desmaële D., Couvreur P., Self-assembly of polyisoprenoyl gemcitabine conjugates: influence of supramolecular organization on their biological activity, *Langmuir* 30 (2014) 6348–6357. <https://doi.org/10.1021/la5007132>

17. Komatsu T., Moritake M., Tsuchida E., Molecular energy and electron transfer assemblies made of self-organized lipid-porphyrin bilayer vesicles, *Chem. Eur. J.* 9 (2003) 4626-4633. <https://doi.org/10.1002/chem.200305013>
18. Lovell J.F., Jin C.S., Huynh E., Jin H., Kim C., Rubinstein J.L., Chan W.C.W., Cao W., Wang L.V., Zheng G., Porphysome nanovesicles generated by porphyrin bilayers for use as multimodal biophotonic contrast agents, *Nat. Mat.* 10 (2011) 324-332. <https://doi.org/10.1038/NMAT2986>.
19. Massiot J., Rosilio V., Ibrahim N., Yamamoto A., Nicolas V., Konovalov O., Tanaka M., Makky A., Newly synthesized lipid-porphyrin conjugates: Evaluation of their self-assembling properties, their miscibility with phospholipids and their photodynamic activity in vitro, *Chem. Eur. J.*, 24 (2018) 19179-19194. <https://doi.org/10.1002/chem.201804865>
20. Bronstein L.-G., Cressey P., Abuillan W., Konovalov O., Jankowski M., Rosilio V., Makky A., Influence of the porphyrin structure and linker length on the interfacial behavior of phospholipid-porphyrin conjugates, *J. Colloids Interface Sci.* 611 (2022) 441-450. <https://doi.org/10.1016/j.jcis.2021.12.114>
21. Bronstein L. G., Toth A., Cressey P., Rosilio V., Di Meo F., Makky A., Phospholipid–porphyrin conjugates: deciphering the driving forces behind their supramolecular assemblies, *Nanoscale*, 14 (2022) 7387-7407. <https://doi.org/10.1039/d2nr01158a>
22. Sharma D., Misba L., Khan A.U., Antibiotics versus biofilm: an emerging battleground in microbial communities, *Antimicrob. Resist. Infect. Control.* 8 (2019) 76. <https://doi.org/10.1186/s13756-019-0533-3>
23. Kim H.-J., Jones M.N., The delivery of benzyl penicillin to *Staphylococcus aureus* biofilms by use of liposomes, *J. Liposome Res.* 14 (2004) 123-139. <https://doi.org/10.1081/LPR-200029887>

24. Rukavina Z., Vanic Z., Current trends in development of liposomes for targeting bacterial biofilms, *Pharmaceutics* 8 (2016) 18. <https://doi.org/10.3390/pharmaceutics8020018>
25. Ambike A., Rosilio V., Stella B., Lepêtre-Mouelhi S., Couvreur P., Interaction of self-assembled squalenoyl gemcitabine nanoparticles with phospholipid-cholesterol monolayers mimicking a biomembrane, *Langmuir* 27 (2011) 4891-4899. <https://doi.org/10.1021/la200002d>
26. Fontaine P., Ciatto G., Aubert N., Goldmann G., Soft Interfaces and Resonant Investigation on Undulator Source: A Surface X-ray Scattering Beamline to Study Organic Molecular Films at the SOLEIL Synchrotron, *Sci. Adv. Mater.* 6 (2014) 2312-2316. <https://doi.org/10.1166/sam.2014.2189>
27. Saoudi L., Girard H.A., Larquet E., Mermoux M., Leroy J., Arnault J.-C., Colloidal stability over months of highly crystalline high-pressure high temperature hydrogenated nanodiamonds in water, *Carbon* 202 (2023) 438-449. <https://doi.org/10.1016/j.carbon.2022.10.084>
28. Kaneshina, S., Ichimori, H., Hata, T., Matsuki, H. (1998). Barotropic phase transitions of dioleoylphosphatidylcholine and stearyl-oleoylphosphatidylcholine bilayer membranes. *Biochim. Biophys. Acta - Biomembr.* 1374 (1998) 1–8. Doi:10.1016/s0005-2736(98)00122-9
29. Koynova R., Caffrey M., Phases and phase transitions of the phosphatidylcholine. *Biochim. Biophys. Acta - Biomembr.* 1376 (1998) 91–145. [https://doi.org/10.1016/S0304-4157\(98\)00006-9](https://doi.org/10.1016/S0304-4157(98)00006-9)
30. Dynarowicz-Latka P., Rosilio V., Boullanger P., Fontaine P., Goldmann M., Baszkin A., Influence of a neoglycolipid and its PEO-lipid moiety on the organization of

- phospholipid monolayers, *Langmuir* 21 (2005) 11941-11948.
<https://doi.org/10.1021/la051749w>
31. Botet-Carreras A., Montero M.T., Domènech O., Borrell J.H., Effect of cholesterol on monolayer structure of different acyl chained phospholipids, *Colloids Surf. B: Biointerfaces*, 174 (2019) 374-383. <https://doi.org/10.1016/j.colsurfb.2018.11.040>
 32. Brezesinski G., Müller H.J., Toca-Herrera J.L., Krustev R., X-ray diffraction and foam film investigations of PC head group interaction in water/ethanol mixtures, *Chem. Phys. Lipids* 110 (2001) 183-194. [https://doi.org/10.1016/S0009-3084\(01\)00135-9](https://doi.org/10.1016/S0009-3084(01)00135-9)
 33. Desroches M.-C., Kasselouri A., Meyniel M., Fontaine P., Goldman M., Prognon P., Maillard Ph., Rosilio V., Incorporation of glycoconjugated porphyrin derivatives into phospholipid monolayers: A screening method for the evaluation of their interaction with a cell membrane, *Langmuir* 20 (2004) 11698-11705.
<https://doi.org/10.1021/la0482610>
 34. Ropers M.-H., Brezesinski G., Lipid ordering in planar 2D and 3D model membranes, *Soft Matter* 9 (2013) 9440-9448. <https://doi.org/10.1039/C3SM51582F>
 35. Hac-Wydro K., Jedrzejek K., Dynarowicz-Latka P., Effect of saturation degree on the interactions between fatty acids and phosphatidylcholines in binary and ternary *Langmuir* monolayers, *Colloids Surf. B: Biointerfaces* 72 (2009) 101-111.
<https://doi.org/10.1016/j.colsurfb.2009.03.019>
 36. Doiron J.E., Le C.A., Bacsa J., Breton G.W., Martin K.L., Aller S.G., Turlington M., Structural consequences of the 1,2,3-triazole as an amide bioisostere in analogs of cystic fibrosis drugs VX-809 and VX-770, *ChemMedChem* 15 (2020) 1720-1730.
<https://doi.org/10.1002/cmdc.202000220>.
 37. Marsh D., Lateral pressure in membranes, *Biochim. Biophys. Acta*, 1286 (1996) 183-223. [https://doi.org/10.1016/s0304-4157\(96\)00009-3](https://doi.org/10.1016/s0304-4157(96)00009-3)

38. Lee A.G., Lipid phase transitions and phase diagrams. I. Lipid phase transitions. *Biochim. Biophys. Acta* 472 (1977) 237-281. [https://doi.org/10.1016/0304-4157\(77\)90018-1](https://doi.org/10.1016/0304-4157(77)90018-1)
39. Ickenstein L.M., Arfvidsson M.C., Needham D., Mayer L.D, Edwards K., Disc formation in cholesterol-free liposomes during phase transition. *Biochim. Biophys. Acta* 1614 (2003) 135-138. [https://doi.org/10.1016/S0005-2736\(03\)00196-2](https://doi.org/10.1016/S0005-2736(03)00196-2)
40. Sreij R., Dargel C., Hannappel Y., Jestin J., Prévost S., Dattani R., Wrede O., Hellweg T., Temperature dependent self-organization of DMPC membranes promoted by intermediate amounts of the saponin aescin, *Biochim. Biophys. Acta*, 1861 (2019) 897-906. <https://doi.org/10.1016/j.bbamem.2019.01.015>

CRedit authorship contribution statement

DC: Methodology, Investigation, Validation; **JPM:** Investigation, Formal analysis;

PF: Methodology, Validation; **JG:** Resources; **FB:** Resources; **VS:** Resources, Supervision;

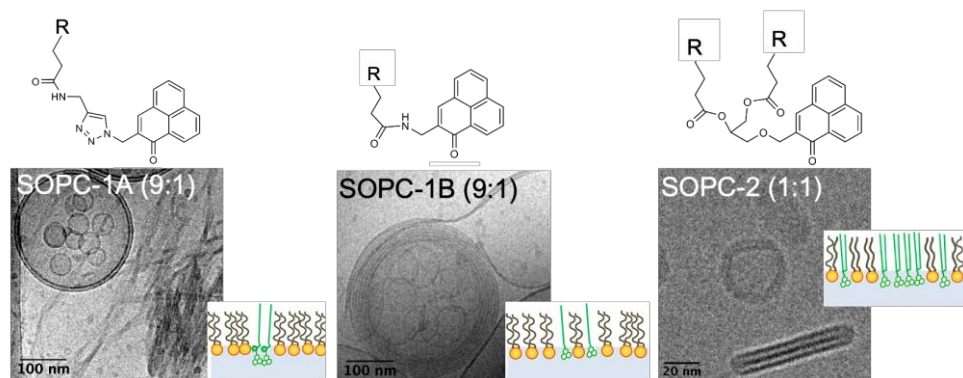
VR: Conceptualization, Methodology, Validation, Supervision, Writing, Review & Editing.

Declaration of interests

The authors declare that they have no known competing financial interests or personal relationships that could have appeared to influence the work reported in this paper.

The authors declare the following financial interests/personal relationships which may be considered as potential competing interests:

Graphical abstract



Highlights

- Phenalenone (PN)-lipid conjugates form various nano-assemblies with phospholipids
- Vesicles containing one-chain PN-lipid transform into bilayer sheets and ribbons
- Vesicles containing two-chain PN-lipid become bilayer discs at high PN molar ratio
- Sheets and discs result from molecule segregation, H-bonding and PN π - π stacking
- PN-lipids control the thermodynamics and structure of nano-assemblies



Click here to access/download
Supplementary Material
Supplementary Material.docx

